


In Vitro Corrosion Behaviour of Ti–6Al–4V and 316L Stainless Steel Alloys for Biomedical Implant Applications

S. Gnanavel¹ · S. Ponnusamy²  · L. Mohan³ · C. Muthamizhchelvan²

Received: 7 September 2017 / Revised: 19 October 2017 / Accepted: 23 October 2017 / Published online: 1 November 2017
© Springer International Publishing AG 2017

Abstract Pulsed laser deposition technique is one of the methods to coat the hydroxyapatite on 316L stainless steel and Ti–6Al–4V implants, which is used in orthopaedics and dentistry applications. In this study, hydroxyapatite (HAP) ceramics in the form of calcium phosphate were deposited on Ti–6Al–4V and 316L stainless steel by the pulsed laser deposition method. The coated thin film was characterised by X-ray diffraction (XRD), scanning electron microscopy with energy-dispersive spectroscopy (EDS) and atomic microscopy. The corrosion studies were carried out on coated and uncoated samples using potentiodynamic polarisation studies in simulated body fluid (Hanks' solution). The bioactivity of the Hap-coated samples on Ti–6Al–4V and 316L stainless steel was evaluated by immersing them in simulated body fluid for 9 days. XRD and EDS analyses confirmed the presence of HAP. The corrosion studies showed that the treated samples have better corrosion resistance compared to Ti–6Al–4V and 316L stainless-steel substrates. The formation of apatite on treated samples revealed the bioactivity of the HAP-coated substrates. HAP-coated Ti–6Al–4V provides higher corrosion protection than the HAP-coated 316L stainless-steel substrates.

Keywords Hydroxyapatite · Pulsed laser deposition · Corrosion · Ti–6Al–4V · 316L stainless steel

✉ S. Ponnusamy
suruponnus@gmail.com

¹ Department of Biomedical Engineering, SRM University, Chennai, Tamilnadu, India

² Center for Materials Science and Nano Devices, SRM University, Chennai, Tamilnadu, India

³ Surface Engineering Division, CSIR-National Aerospace Laboratories, Bangalore, Karnataka, India

1 Introduction

Titanium and stainless steel are most commonly preferred materials for orthopaedics and dentistry applications. Their mechanical and corrosion resistance properties were more reasonable properties to enhance the orthopaedics and dental. However, the poor wear resistance of Ti-based alloys causes some limitations in the long-term use of Ti in bio-implants. Over the past decade, different types of surface modification techniques have been developed to improve the wear resistance of stainless steel and Ti-based alloy [1–4]. The clinical advantage of HAP-coated implants has been established through several methods [5–7]. From this, plasma spray is the only commercially available method currently for coating the implant materials using calcium phosphates, especially for hydroxyapatite (HAP) [8, 9]. However, the plasma-sprayed HAP coatings demonstrate the certain detriments in the clinical applications, such as low adherence on the metal surface and the absence of consistency in morphology and crystallinity [10, 11]. Pulsed laser deposition (PLD) technique has been proposed as a promising and alternate for coating of titanium and stainless-steel implants with hydroxyapatite [8, 9, 12]. The main advantage of PLD technique is the ability to deposit uniform, pure, crystalline and stoichiometric hydroxyapatite films [13] and also PLD allows for controlling the surface properties of the substrate layer. Knowledge of the residual stresses (RS) induced in the coating and the substrate during deposition is essential in predicting the location of failures [14–17]. Therefore, the laser ablation technique or pulsed laser deposition (PLD) is an alternate technique available to obtain a thin layer of coating over a metallic substrate. The PLD technique is directed towards the creation of highly crystalline apatite films at various substrate temperatures [18]. The limited work was available on Ti–6Al–4V and 316L stainless steel by pulsed

laser deposition. The deposition of HAP on Ti–6Al–4V and 316L stainless steel by PLD is limited, and its studies on corrosion are lack in the literature.

In the present work, pure ceramics HAP coated with Ti–6Al–4V and 316L stainless-steel substrates by using the pulsed laser deposition (PLD) technique.

2 Materials and Methods

2.1 Sample Preparation

Titanium alloy (Ti–6Al–4V) and 316L stainless-steel (10×10×2 mm) test samples with the dimension of 10×10×2 mm were ground with silicon carbide paper at various grades and polished using by 0.1 μm size diamond paste. The prepared samples were cleaned using acetone by ultrasonication for 15 min. The cleaned sample was dried 15 min at room temperature.

2.2 Pulsed Laser Deposition (PLD)

The deposition was carried out in a custom-designed spherical chamber that contains the target and substrate holders confronting each other, along with a beam of laser focusing optical lens assembly and gas inlet port. Extra windows port was obtained for optical emission analysis. The target holder can carry many targets, each of which could be rotated eccentrically for uniform erosion using externally mounted motor and gears. The substrate holder was attached to a concealed heater with a shutter in the front. An external PID controller fuelled the radiator so that the substrate temperature could be kept up at the required temperature. A side window at 135° angle from the target holder port was used to mount the focusing assembly for the laser beam. The target selection, rotation, shutter position and laser beam were controlled using a microprocessor-based remote control unit. The hydroxyapatite targets were made from a suspension of HAP powder by Sigma-Aldrich company. These HAP nanopowders were compressed to 800 bars in a cold isostatic press and sintered at 900 °C for 8 h. After it was structured to a circular shape and mounted on the target holder [1], Nd: YAG pulsed laser (Quanta-Ray, Spectra-Physics) operating at 355 nm, 10 Hz repetition rate, was used for the ablation. The laser beam was directly focused on the HAP target at an incidence angle of 45°. The target was rotated during the deposition. The target and chamber were kept at ground potential. Titanium alloy Ti–6Al–4V and 316L stainless steel were used as substrates. The target–substrate distance was held at 4 cm, and the shutter was kept closed. The chamber was tapped down to a pressure of 10^{−5} mbar using a diffusion pump backed by the

rotary pump. After stabilising at the base pressure, pure, dry nitrogen gas was admitted via a mass flow controller to bring the pressure to ~ 10^{−3} mbar. The laser power obtained was set at 3 J/cm². The coatings were carried out for 60 min. In the case of sample thickness measurement, surface masking was done by up to the middle portion. Thickness of the coating was around 1 μm achieved. The coated substrates were taken out after cooling down.

2.3 Characterisation Technique

The surface morphology and element composition of the sample were examined by field emission scanning electron microscopy (FESEM—Supra 40 VP Carl Zeiss, Germany). Atomic force microscopy was performed with Easy scan2, Nanosurf, Switzerland. The phases formed in the nanocomposite coatings were investigated by X-ray diffraction (XRD) using PHILIPS X-ray diffractometer (BRUKER, Germany). A monochromatic source, CuKα radiation ($\lambda = 0.1548$ nm) was applied, and the samples were scanned from 20° to 70° at a scanning rate of 0.5°/min.

2.4 Immersion Studies

Immersion studies were carried out for substrate and treated samples by immersing them for 9 days at 37 °C in 40 ml of freshly prepared simulated body fluid (SBF) Hanks' solution with ion concentrations almost equivalent to that of human blood plasma (Na⁺ = 142.0, K⁺ = 5.0, Mg²⁺ = 1.5, Ca²⁺ = 2.5, HCO^{2−} = 4.2, HPO₄^{2−} = 1.0, SO₄^{2−} = 0.50 and Cl[−] = 147.96 mM). The chemical composition of Hanks' solution is as follows: 0.185 g CaCl₂, 0.4 g KCl, 0.06 g KH₂PO₄, 0.1 g MgCl₂·6H₂O, 0.1 g MgSO₄·7H₂O, 8.0 g NaCl, 0.35 g NaHCO₃, 0.48 g Na₂HPO₄ and 1.00 g D-glucose in 1 L of Mill-Q water [19]. The pH of the arrangement was maintained from 7.2 to 7.6, and test was performed at 37 °C.

2.5 Electrochemical Measurements

Potentiodynamic polarisation investigations of the sample were carried out using CHI604D electrochemical workstation supplied by CH Instruments, USA. The traditional three-electrode glass cell was utilised to complete the electrochemical studies. The test was performed in 200 ml of Hanks' solution. The test sample was kept as a working electrode; platinum foil and saturated calomel anode (SCE) were utilised as counter and reference electrodes, respectively. The specimen was immersed in the Hanks' solution for 60 min to attain the stability.

3 Results and Discussion

3.1 XRD Analysis

The crystalline structure of Ti-6Al-4V and 316L stainless steel was analysed by X-ray diffraction pattern. CuK α radiation ($\lambda = 0.1548$ nm) was applied, and the samples were scanned from 20° to 70° at a scanning rate of 0.5°/min. The phases formed on the surface of HAP-coated Ti-6Al-4V and 316L stainless steel were investigated using XRD analysis and are illustrated in Fig. 1. The XRD patterns of the 316L stainless steel of calcium phosphate (CaP) are in consonance with JCPDS#00-003-0429. The peaks at 27.02°, 20.38°, 24.33° and 39.39° confirm the presence of the calcium phosphate; similarly, the XRD patterns of the Ti-6Al-4V of CaP are in consonance with JCPDS#01-086-1585. The peaks at 44.25°, 45.21°, 48.63° and 60.20° confirm the presence of the calcium phosphate. The presence of calcium phosphate in the coating mimics the bone composition and gives an added advantage because it leads to enhanced osseointegration. The elemental composition of 316L stainless steel for Fe, Ni and Cr confirms with JCPDS No: 96-500-0218, 96-901-3035 and 01-088-2323. The particle size of the HAP-coated 316L stainless steel and Ti was calculated using Scherrer's formula,

$$d = 0.9\lambda/\beta \cos \theta$$

where λ —wave length of X-rays, β —FWHM of diffraction peak and θ —angle corresponding to the peaks. The particle size of the HAP-coated 316L stainless steel and Ti alloy was 19.79 nm and 19.77 nm, respectively.

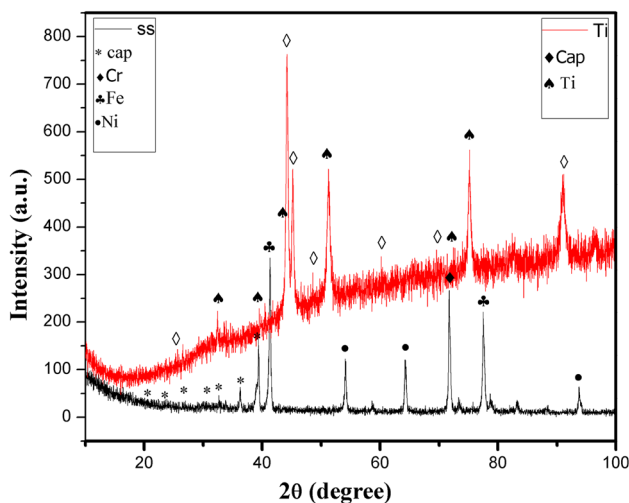


Fig. 1 X-ray diffraction pattern of HAP-coated 316L stainless steel and Ti-6Al-4V alloy

3.2 Morphology Analysis

The surface morphology of the coated HAP thin film was analysed by using field emission scanning electron microscope (FESEM) at different magnifications (X3000, X12000) and is shown in Fig. 2. In the figure (a1, a2) represents the HAP-coated 316L stainless steel, and (b1, b2) represents the HAP-coated titanium alloy. FESEM micrographs reveal the formation of a uniform coating with no cracks in the HAP-coated sample on titanium alloys and 316L stainless steel. From the figure, the spherical-like morphology of HAP can be seen on the surface of Ti-6Al-4V and 316L stainless steel with the average size extent from 5 to 10 μ m. They have a dense layer formed by grains of different sizes on which droplets are uniformly distributed. The HAP coatings present a particular morphology similar to those obtained with a ruby laser [20–22]. However, in biomedical applications, excess surface particles are desirable because they cause an extension of the surface and increase osseointegration, cell growth and proliferation, which are the major aims of HAP coatings on Ti-6Al-4V and 316L stainless steel. The surface topography of the HAP-coated Ti-6Al-4V and 316L stainless-steel alloys was analysed using an atomic force microscope (AFM), as shown in Fig. 3. The estimated average surface roughness (Ra) values of HAP coated on Ti-6Al-4V metal 316L stainless steel are 27.35 nm and 82.75 nm, respectively.

The elemental composition of the Hap-coated surface examined by EDS is shown in Fig. 4a and b. The peaks corresponding to Ca, P and O revealed the presence of Hap along with small amount of Ti, Fe, Cr, Ni and C corresponds to substrate materials. The atomic and weight percentage of HAP-coated 316L stainless steel and Ti-6Al-4V alloy are presented in Tables 1 and 2. From tables, the estimated Ca/P ratio is 2.25, 1.96 for stainless steel and titanium alloy, respectively.

3.3 In Vitro SEM Analysis

Figure 5a and b shows FESEM images of HAP-coated samples of Ti-6Al-4V and 316L stainless-steel surfaces after 9-day immersion in SBF, with an ionic concentration equal to that of human blood plasma. From the figure, the growth of the HAP was confirmed on the surface of the coating after immersion for 9 days in SBF solution. The immersion in SBF HAP-coated substrate presents a specific morphology similar to that of reported by G.P.Dinda et al. [23]. The growing rate of HAP-coated titanium alloys and 316L stainless steel on the surface of the coating is notably increased after immersion. However, a few minor cracks can be seen in the coatings. These cracks developed during annealing of the coatings but were not due to the immersion in the SBF.

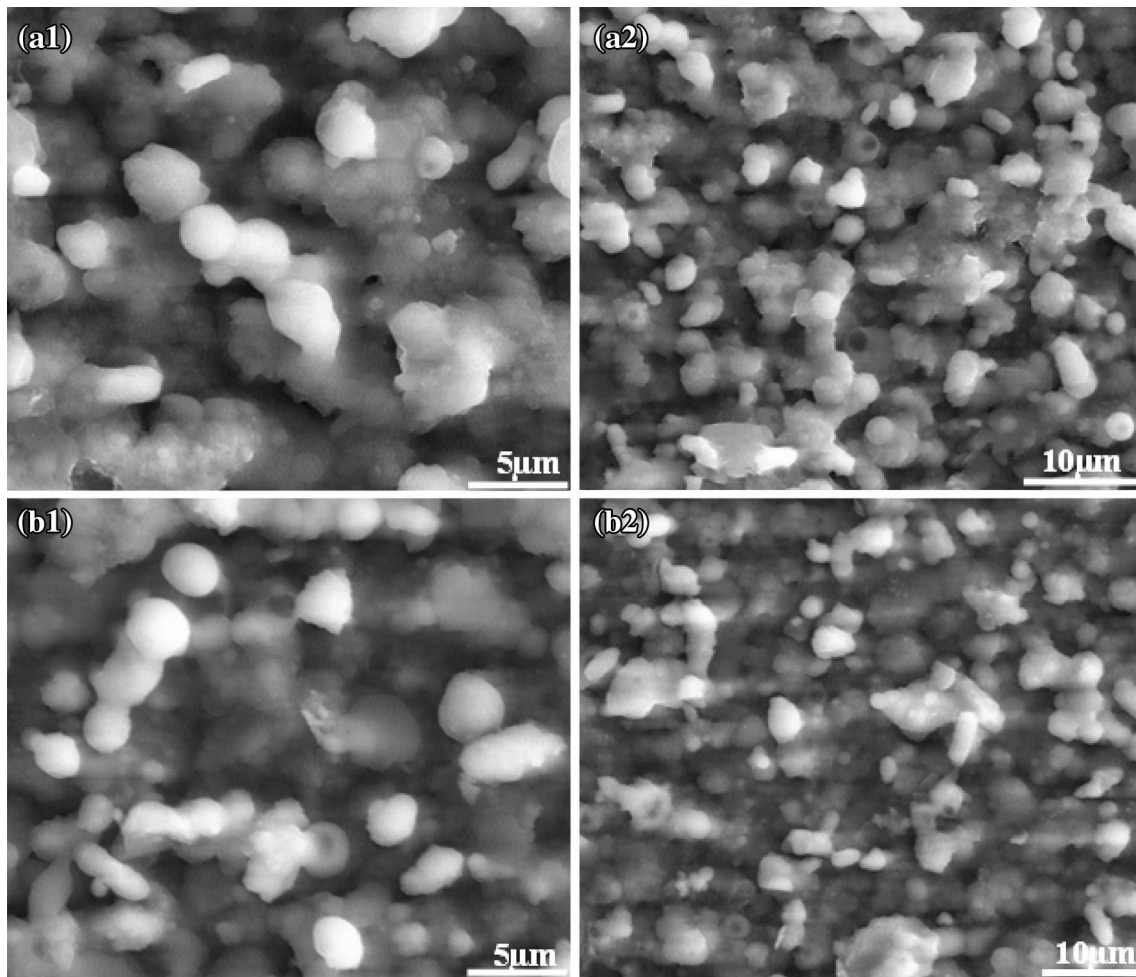


Fig. 2 SEM image HAP-coated **a1, a2** 316L stainless steel and **b1, b2** Ti-6Al-4V substrate

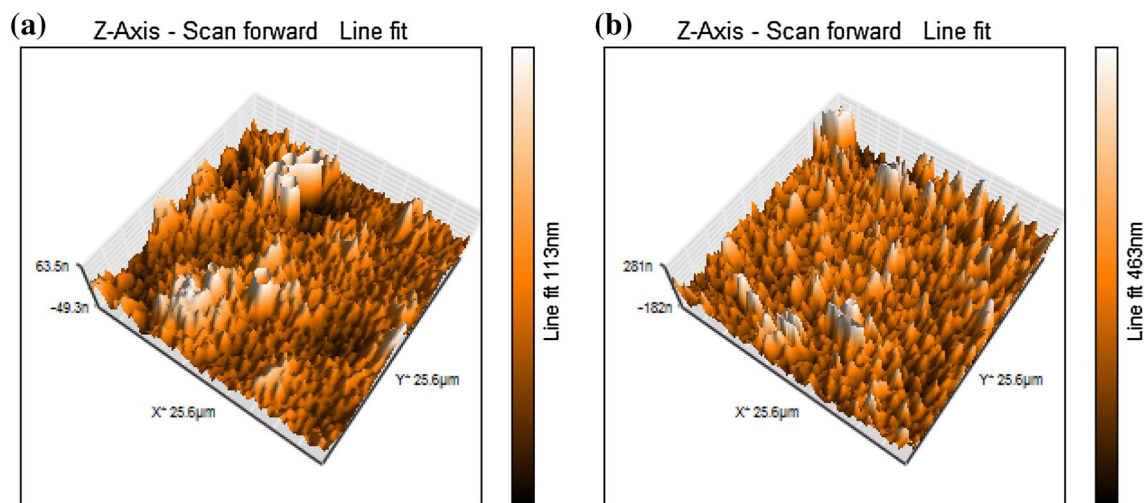


Fig. 3 AFM images of samples **a** HAP-coated 316L stainless steel, **b** HAP-coated Ti-6Al-4V sample

Fig. 4 EDS spectra of HAP-coated samples **a** Ti–6Al–4V, **b** 316L stainless steel

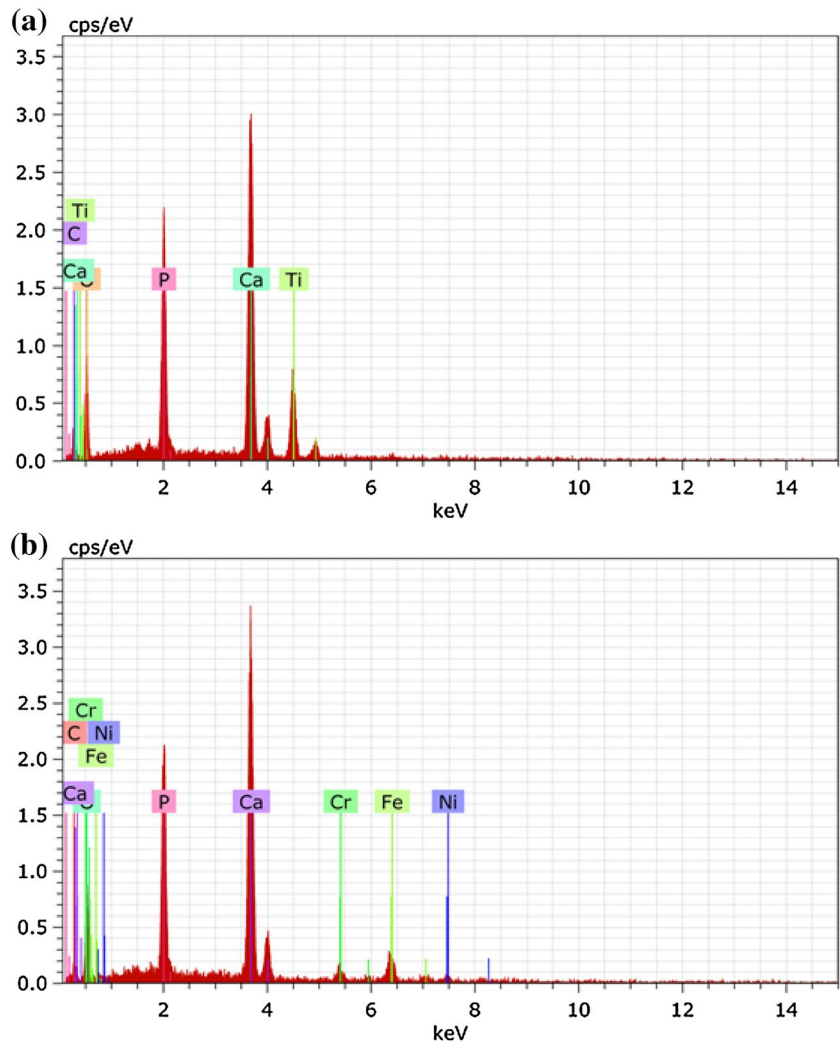


Table 1 EDS analysis for 316L stainless-steel HAP-coated alloys

Elements	Atomic number	Weight%	Atomic%	Error sigma weight%
O	8	35.54	53.24	8.46
Ca	20	34.75	20.78	1.12
P	15	11.88	9.20	0.54
Fe	26	8.24	3.54	0.44
C	6	79.11	11.56	2.77
Cr	24	2.51	1.16	0.21
Ni	28	1.30	0.53	0.18

Table 2 EDS analysis for Ti–6Al–4V alloys HAP-coated alloys

Elements	Atomic number	Weight%	Atomic%	Error sigma weight%
O	8	37.62	50.74	8.66
Ca	20	28.72	15.46	0.97
C	6	11.64	20.92	3.71
P	15	11.29	7.87	0.54
Ti	22	10.22	4.61	0.43
Al	13	0.51	0.41	0.09

3.4 In Vitro EDS Analysis

Figure 6 shows the EDS results of HAP-coated 316L stainless steel and Ti–6Al–4V after immersed in Hanks’ solution. The presence of Ca, P and O confirms the formation of HAP layer on the 316L stainless steel and Ti–6Al–4V after PLD deposition of Hap. Further, after 9 days immersion,

samples show the marginal increase in Ca, P and O percentage, which confirm the formation of apatite layer on the surface. The calculated Ca/P ratio of the Hap coated in SBF solution was 2.34 and 2.09 for stainless steel and titanium alloys, respectively. When compared with in vitro SBF Hap-coated alloys, Ca/P ratio has marginally increased than the Hap-coated alloys [24]. These results show that the in vitro Hap-coated alloys have good osseointegration.

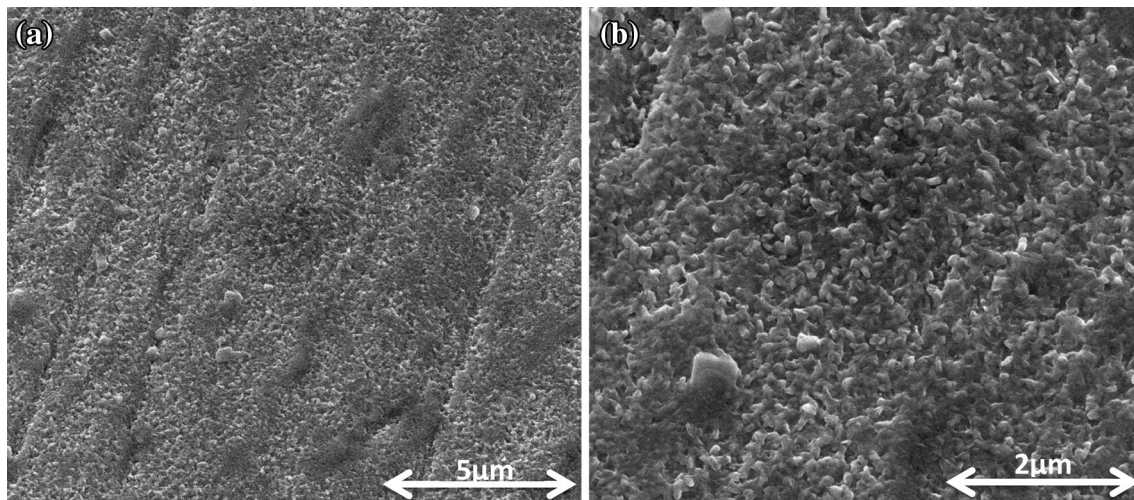
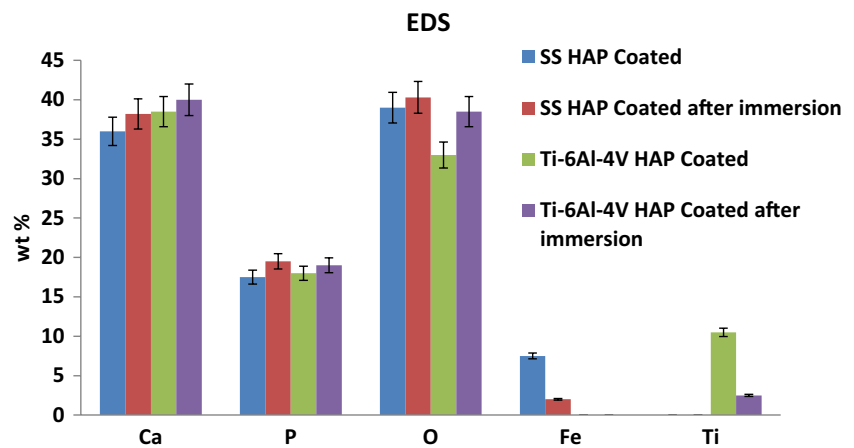


Fig. 5 FESEM images of in vitro solution **a** 316L stainless steel, **b** Ti-6Al-4V substrate

Fig. 6 EDS results of HAP-coated 316L stainless steel and Ti-6Al-4V after immersion in SBF solution



3.5 Corrosion Analysis

The potentiodynamic polarisation curves of the substrate and HAP-coated samples (Ti-6Al-4V and 316L stainless steel in Hanks' solution (pH is between 7.2 and 7.6) are presented in Fig. 7. The electrochemical parameters, namely corrosion potential (E_{corr}) and corrosion current density (i_{corr}), acquired for the substrate and treated samples are given in Table 3. The polarisation resistance, R_p , was assessed from the anodic and cathodic slopes and is also listed in Table 3. From the table, it is observed that the i_{corr} acquired for the treated samples is 0.007 and 0.003 $\mu\text{A}/\text{cm}^2$ for 316L stainless steel and Ti-6Al-4V samples, respectively.

Additionally, from the table, the polarisation resistance is found around to be $1.2 \times 10^7 \Omega \text{ cm}^2$ for the Ti-6Al-4V treated specimen, which is higher than that for 316L stainless-steel substrate and treated samples. The E_{corr} values moved to more positive value on Ti-6Al-4V and 316L stainless-steel coated samples. From this result, it is concluded

that the Ti-6Al-4V HAP-coated alloys have better corrosion resistance when compared with that of the HAP-coated 316L stainless steel [25]. These outcomes showed that the HAP-coated Ti-6Al-4V combination has better corrosion resistance when compared with that of the 316L stainless steel (Fig. 7).

4 Conclusion

Since, individual HAP coatings have already proved to be biocompatible and provide higher osseointegration, an effort has been made to produce HAP coatings by PLD on Ti-6Al-4V and 316L stainless steel. Various techniques characterised the coated samples and tested for their corrosion resistance. The following conclusions were drawn from the above experimental evidence. The structural analysis is carried out using XRD, and it is demonstrated that as-deposited material is in the crystalline nature of

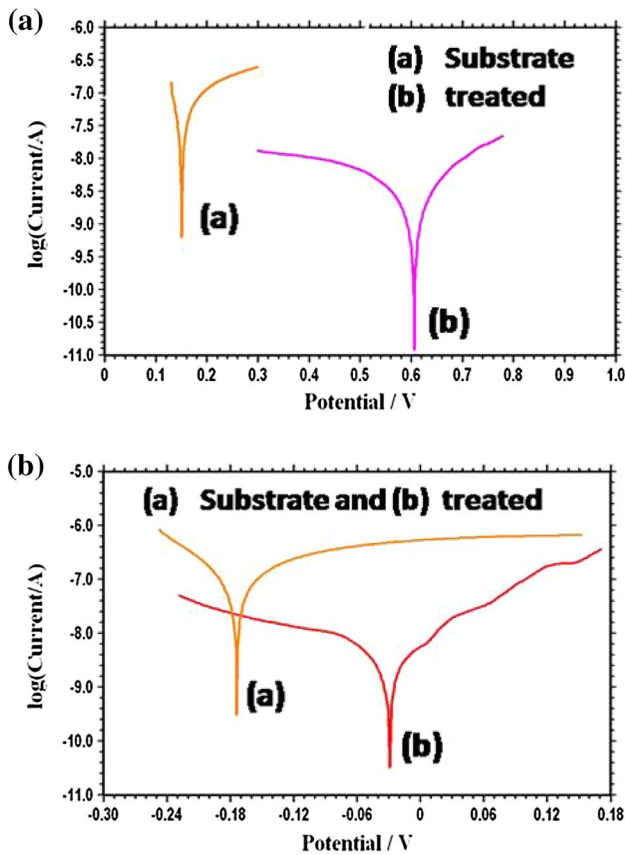


Fig. 7 Potentiodynamic polarisation curves **a** 316L stainless steel, **b** Ti-6Al-4V substrate

HAP. The morphology of the HAP-coated titanium alloy and 316L stainless steel has studied by using FESEM, and the measure of the spherical structure is obtained inside of extent from 5 to 10 μm. It has likewise been shown that the hydroxyapatite improves the attachment of the covering to the substrate mostly. The HAP-coated 316L stainless steels are high corrosion current and corrosion rate, when compared with HAP-coated Ti-6Al-4V. This can be considered as titanium alloy which is preferred use over 316L stainless steel. Therefore, HAP-coated Ti-6Al-4V provides higher corrosion protection than the HAP-coated

Table 3 Potentiodynamic polarisation results of substrate and treated samples

S. no.	Sample	E_{corr} (V)	i_{corr} ($\mu\text{A}/\text{cm}^2$)	R_p ($\Omega \text{ cm}^2$)
1	Ti-6Al-4V substrate	0.150	0.013	2.6×10^6
2	Ti-6Al-4V treated sample	0.606	0.003	1.2×10^7
3	316L stainless-steel substrate	-0.174	0.095	1.7×10^5
4	316L stainless-steel treated sample	-0.029	0.007	5.2×10^6

316L stainless-steel substrates, which can be used for bio-medical implant applications.

Acknowledgements The author acknowledges the Centre for Nanoscience and Nanotechnology, SRM University for using the laboratory facilities. Author would like to thank Mr. Murali, NRC, SRM University for FESEM studies, and Mr. Bijo Joseph, Department of Physics and Nanotechnology, SRM University for XRD analysis.

References

1. Wang RR, Welsch GE, Monteiro O (1999) Silicon nitride coating on titanium to enable titanium-ceramic bonding. *Biomed Mater Res* 46:2-262
2. Kuo MC, Yen SK (2002) The process of electrochemical deposited hydroxyapatite coatings on biomedical titanium at room temperature. *Mater Sci Eng* 20:153-160
3. Thian ES, Khor KA, Loh NH, Tor SB (2001) Processing of HA-coated Ti-6Al-4V by a ceramic slurry approach: an in vitro study. *Biomaterials* 22:1225-1232
4. Lynn AK, DuQuesnay DL (2002) Hydroxyapatite-coated Ti-6Al-4V: part 1: the effect of coating thickness on mechanical fatigue behavior. *Biomaterials* 23:1937-1946
5. Klein C, Pratkan P, van der Lubbe HB, Wolke JG, de Groot K (1991) Plasma sprayed coatings of tetracalciumphosphate, hydroxylapatite and alpha tricalciumphosphate on titanium alloy: an interface study. *J Biomed Mater Res* 25:53-65
6. Ducheyne P, Breight J, Cuckler J, Evans B, Radin S (1990) Effect of CaP coating characteristics on early post-operative bone tissue ingrowth. *Biomaterials* 11:531-540
7. Tisdell CL, Golberg VM, Parr JA, Bensuan JS, Staikoff LS, Stevenson S (1994) The influence of HA and TCP coating on bone growth into titanium fiber-metal implants. *J Bone Joint Surg Am* 76:159-171
8. Nelea V, Mihailescu IN, Jelinec M (2007) Biomaterials: new issues and breakthroughs for biomedical applications. In: Eason R (ed) *Pulsed laser deposition of thin films*. Wiley, New Jersey
9. Koch CF, Johnson S, Kumar D, Jelinec M, Chrisey DB, Doraiswamy A, Jin C, Narayan RJ, Mihailescu IN (2007) Pulsed laser deposition of hydroxyapatite thin films. *Mater Sci Eng* 27:484-494
10. Garcíya-Sanz FJ, Mayor MB et al (1997) Hydroxyapatite coatings: a comparative study between plasma-spray and pulsed laser deposition techniques. *J Mater Sci Mater Med* 8:861-865
11. Fazan F, Marquis PM (2000) Dissolution behavior of plasma-sprayed hydroxyapatite coatings. *J Mater Sci Mater Med* 11:787-793
12. Bao Q, Chen C, Wang D, Ji Q, Lei T (2005) Pulsed laser deposition and its current research status in preparing hydroxyapatite thin films. *Appl Surf Sci* 252:1538-1544
13. Mihailescu IN, Torricelli P et al (2005) Calcium phosphate thin films synthesized by pulsed laser deposition: physico-chemical characterization and in vitro cells response. *Appl Surf Sci* 248:344-348
14. Yang YC, Chang E (2001) Influence of residual stress on bonding strength and fracture of plasma-sprayed hydroxyapatite coatings on Ti-6Al-4V substrate. *Biomaterials* 13:1827-1836
15. Yang YC, Chang E, Hwang BH, Lee SY (2000) Biaxial residual stress states of plasma-sprayed hydroxyapatite coatings on titanium alloy substrate. *Biomaterials* 21:1327-1337
16. Sergio V, Sbaizero O, Clarke DR (1997) Mechanical and chemical consequences of the residual stresses in plasma sprayed hydroxyapatite coatings. *Biomaterials* 18:477-482

17. Tsui YC, Doyle C, Clyne TW (1998) Plasma sprayed hydroxyapatite coatings on titanium substrates part 1: mechanical properties and residual stress levels. *Biomaterials* 19:2015–2029
18. Fernandez-Pradas JM, Sardin G et al (1998) Hydroxyapatite thin films by excimer laser ablation. *Thin Solid Films* 317:393–396
19. Mohan L, Dilli Babu P, Kumar Prateek, Anandan C (2013) Influence of zirconium doping on the growth of apatite and corrosion behavior of DLC-coated titanium alloy Ti–13Nb–13Zr. *Surf Interface Anal* 45:1785–1791
20. Baeri P, Torrisi L, Marino N, Foti G (1992) Ablation of hydroxyapatite by pulsed laser irradiation. *Appl Surf Sci* 54:210–214
21. Koch C et al (2007) Pulsed laser deposition of hydroxyapatite thin films. *Mater Sci Eng C* 27(3):484–494
22. Torrisi L (1994) Structural investigations on laser deposited hydroxyapatite films. *Thin Solid Films* 237:1–2
23. Dinda GP, Shin J, Mazumder J (2009) Pulsed laser deposition of hydroxyapatite thin films on Ti–6Al–4V: effect of heat treatment on structure and properties. *Acta Biomater* 5:1821–1830
24. Fernandez-Pradas JM, Serraa P, Morenzaa JL, De Azab PN (2002) Pulsed laser deposition of pseudowollastonite coatings. *Biomaterials* 23:2057–2061
25. Anandan C, Mohan L (2013) In vitro corrosion behavior and apatite growth of oxygen plasma ion implanted titanium alloy β -21S. *JMEPEG*. <https://doi.org/10.1007/s11665-013-0628-6>